JOURNAL OF PROPULSION AND POWER
Vol. 19, No. 4, July–August 2003

Characteristics of Liquid Film and Spray Injected from Swirl Coaxial Injector

Takao Inamura*
Hirosaki University, Hirosaki 036-8561, Japan
and
Hiroshi Tamura† and Hiroshi Sakamoto‡
National Aerospace Laboratory, Kakuda 981-1525, Japan

The liquid film flow on the inner wall of the center post of a swirl coaxial injector was analyzed theoretically. The development of the boundary layer in the liquid-film flow and the transition from laminar to turbulence were studied. The film thickness at the post exit was measured using a contact needle probe, and the predicted film thickness was compared with the measurements. The film thickness varies in the azimuthal direction due to the geometry of the liquid inlet. The average film thickness at the post exit increases as the post length increases. The sheet cone angle and breakup length were measured using photography and a contact mesh probe, and their empirical equations were deduced by modifying those of a simplex swirl injector, taking into account the liquid momentum loss due to a long center post. These equations predict the sheet cone angle and breakup length well, except for small liquid flow rates. The mean droplet size and droplet velocity were measured by a phase Doppler particle analyzer. The measured spray characteristics exhibited characteristics similar to those of a conventional airblast atomizer.

Nomenclature

A	=	constant in Eq. (25)
a	=	constant in Eq. (43)
B	=	constant in Eq. (48)
b	=	constant in Eq. (43)
C_1	=	constant in Eq. (32)
C_2	=	constant in Eq. (35)
C_3	=	constant in Eq. (39)
d_c	=	diameter of gas core at liquid inlet as shown in Fig. 3
d_e	=	exit diameter of center post as shown in Fig. 3
h	=	liquid film thickness
h_i	=	liquid film thickness at liquid inlet
h_0	=	liquid film thickness at center post exit
$\bar{h}$	=	average liquid film thickness
K	=	atomizer constant, equal to the ratio of sectional area of inlet to outlet of center post
k	=	cavity factor, d_c/d_e
L	=	length of center post as shown in Fig. 3
L_{bu}	=	breakup length of injected liquid film
L_x	=	distance along streamline defined by Eq. (47)
m	=	mass flow rate
P	=	injection pressure
p	=	variable defined by Eq. (45)
Q	=	liquid flow rate per unit width
q	=	variable defined by Eq. (46)
Re	=	Reynolds number defined by Eq. (17)
Re_x	=	boundary Reynolds number defined by Eq. (13)
$Re_{x\,\mathrm{crit}}$	=	critical boundary Reynolds number from laminar to turbulent
r	=	radial distance from spray axis
U	=	liquid surface velocity in axial direction
U_a	=	average liquid axial velocity
U_d	=	average droplet velocity
U_i	=	constant liquid axial velocity at $x = 0$
U_0	=	liquid injection velocity at center post exit
u	=	liquid axial velocity
v	=	liquid radial velocity
x	=	coordinate as shown in Fig. 3
x_t	=	x at point where transition of boundary layer from laminar to turbulent occurs
x_0	=	x at point where laminar boundary layer reaches film surface
y	=	coordinate as shown in Fig. 3
Z	=	axial distance from injector exit
α	=	sheet cone angle at $x = 0$
α_R	=	sheet cone angle at $x = L$
δ	=	thickness of boundary layer
ζ	=	wave amplitude at liquid film breakup
ζ_0	=	initial wave amplitude
η	=	nondimensional coordinate in y direction
θ	=	azimuthal angle
ν	=	kinetic viscosity
ξ	=	distance in azimuthal direction as shown in Fig. 4
ρ	=	density
σ	=	surface tension
τ_w	=	wall shear stress

Subscripts

g	=	gas
l	=	liquid

Superscript

*	=	nondimensional variable

Received 16 September 2001; revision received 27 February 2003; accepted for publication 6 March 2003.

*Professor, Faculty of Science and Technology. Member AIAA.
†Group Leader, Advanced Nozzle Group, Rocket Propulsion Center. Senior Member AIAA.
‡Senior Researcher, Advanced Nozzle Group, Rocket Propulsion Center.

I. Introduction

In many liquid oxygen/hydrogen rocket engines, coaxial injectors are used because of their simple structure and good performance. However, the extent to which the injector size can be increased to maintain good spray characteristics is limited. Thus, an increase of the engine size implies an increase in the number of injectors, resulting in an increase of cost. To reduce the number of injectors, it is necessary to employ an atomizing liquid-sheet injector, for instance, a swirl injector.

Swirl coaxial injectors have recently been investigated for use in reusable rocket engines.[1–3] This type of injector has the same structure as conventional swirl injectors commonly employed in gas turbine engines, but does not employ gas injection. A liquid is introduced into a center post tangentially, and a conical sheet is formed at the exit of the post. The design of a swirl coaxial injector differs from that of a conventional swirl injector in that the length of the center post is much longer due to the existence of a hydrogen manifold. As a result, the spray characteristics deteriorate because of the momentum loss.

The liquid-film thickness at the injector exit is one of the major factors determining the spray droplet size. Rizk and Lefebvre experimentally established a relationship between the liquid-film thickness at the atomizer exit and the spray droplet size in a coflow-type airblast atomizer.[4] Inamura and Nagai deduced an empirical correlation for impinge-type airblast atomizers.[5] A close relationship between the film thickness and the droplet size was established. In this paper, the liquid flow on the inner wall of the center post of a swirl coaxial injector was investigated theoretically. The predicted film thickness at the post exit was compared with measurements. Empirical equations of the sheet cone angle and breakup length were deduced in the absence of the gasstream. Finally, the mean droplet size and droplet velocity were measured by a phase Doppler particle analyzer.

II. Experimental Apparatus and Conditions

The swirl coaxial injector under consideration is shown in Fig. 1. Liquid is introduced tangentially into the center post through three holes, each with a diameter of 0.81 mm. The liquid flows spirally toward the exit, and the swirling film along the inner wall of the center post creates a gas core, except at a very small liquid flow rate. The film exits the tube in the form of a hollow cone sheet due to the swirling motion. The high-speed gasstream is injected axially through the annular slit surrounding the center post and impinges on the conical liquid sheet. The present work, however, does not include the external gasstream to focus on the fundamental behavior of the liquid film.

The behavior of the hollow cone sheet issued from the injector exit was observed by a backlighted photograph. The film thickness at the injector exit was measured by the contact needle method.[6] The fundamentals of this method are shown in Fig. 2. An electric voltage of 15 V is applied between the needle and the liquid film. When the needle touches the film, the electric circuit is closed, and a voltage difference across the resistance is produced and is measured by a voltmeter. The contact needle attached to a micrometer head is coated with insulation paint, except for its tip, to prevent erroneous detection of a liquid film. The accuracy of the needle positioning is 1 μm. Because the liquid-film surface fluctuates, the signal detected by the voltmeter also fluctuates. In the present study, the radial position where the ratio of the closed-circuit time to the measurement time becomes 50% was regarded as the position of the film surface. The accuracy of the thickness measurement of the still liquid film was within 10 μm. The experimental repeatability was within 50 μm throughout all of the measurements.

The breakup length of the sheet was measured by the contact mesh method, as detailed in Ref. 7. The fundamentals of the method are the same as those of the contact needle method, except that a mesh, rather than a needle, is used to probe the film. The mesh is mounted on a translation stage, and the accuracy of the mesh positioning is 0.1 mm.

The droplet size and velocity were measured by a phase Doppler particle analyzer (Dantec Company, 10-mW He–Ne laser). The experimental conditions are summarized in Table 1. Water and gaseous nitrogen were employed as the atomizing liquid and gas, respectively.

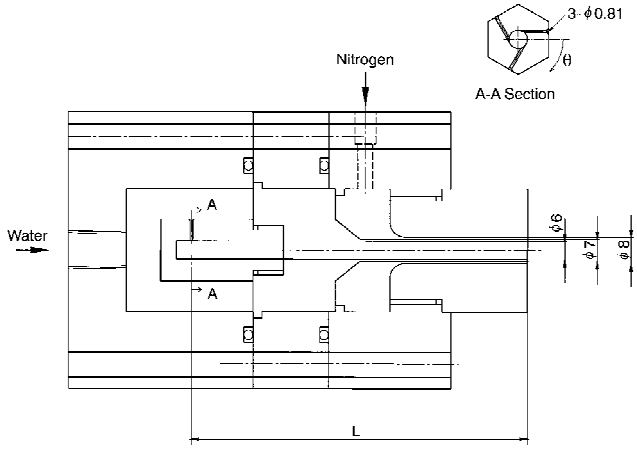

Fig. 1 Schematic diagram of swirl coaxial injector (millimeters).

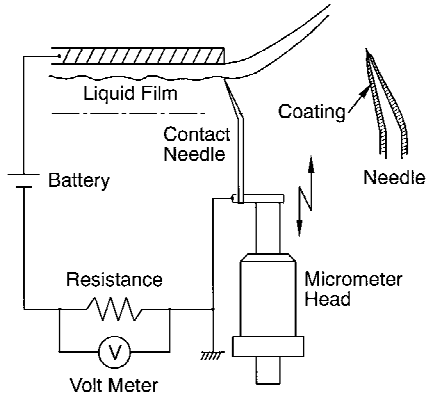

Fig. 2 Contact needle method.

III. Theoretical Analysis of Film Thickness

The film thickness at the injector exit is one of the major factors that govern the spray characteristics and is an important parameter for the design of an injector. In the present study, the liquid-film thickness was analyzed theoretically. The coordinate system and the variables are defined in Fig. 3. The following assumptions are made.

1) The liquid flow is two dimensional (planar). Essentially, a three-dimensional analysis should be done. However, in the present

Table 1 Experimental conditions

Parameter	Value
Liquid mass flow rate m_l	10.0–48.0 g/s
Liquid injection pressure P_l	0.033–0.7 MPa
Gas mass flow rate m_g	2.0–6.0 g/s
Gas injection pressure P_g	0.13–0.25 MPa
Length of center post tube L	50, 70, 100 mm

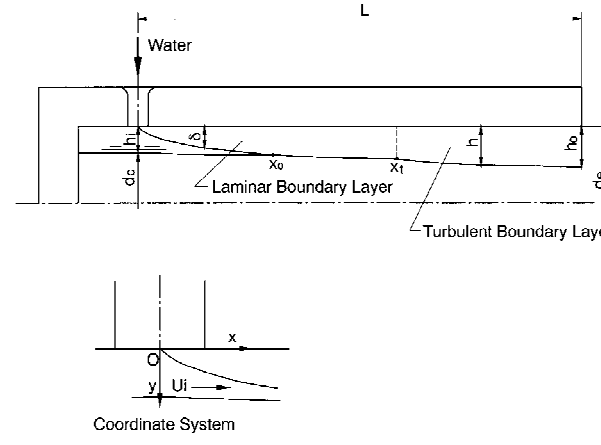

Fig. 3 Coordinate system and variables.

study the two-dimensional (planar) analysis was employed because of the rapid decline of a liquid velocity in an azimuthal direction due to the wall friction and the simplicity of the analysis. A correctional factor can be introduced, if necessary.

2) A laminar boundary layer originates at $x = 0$.

3) The velocity distribution in the laminar boundary layer can be approximated by the biquadratic equation of Ishigai et al.[8] and the distribution in the turbulent boundary layer by the one-seventh power law.

4) The liquid velocity outside the laminar boundary layer can be approximated by a constant value U_i.

5) The effect of the surrounding gas and gravity on the liquid-film behavior can be ignored. The pressure gradient along the streamline can be ignored.

6) The liquid velocity U_i and the liquid-film thickness h_i at $x = 0$ (Fig. 3) can be determined using the potential flow theory proposed by Tanasawa and Kobayasi.[9]

7) The momentum of the liquid film is conserved at transition from the laminar to the turbulent boundary layer.

Tanasawa and Kobayasi[9] analyzed the liquid flow in a swirl atomizer by assuming a potential flow and deduced a liquid-film thickness and a sheet cone angle at the atomizer exit. Results were expressed in terms of an atomizer constant that depended on the atomizer geometry.[9] Rizk and Lefebvre analyzed the internal flow of a simplex swirl atomizer.[10] The liquid viscosity was taken into account. They expressed the sheet cone angle as a function of the pressure drop along the discharge orifice and the liquid-film thickness at the atomizer exit as the injection pressure differential across the atomizer. In the present study, to define the injection pressure differential across the injector and the pressure drop along the discharge orifice is difficult because of the much longer swirl chamber compared to conventional swirl atomizers. Consequently, the potential flow theory proposed by Tanasawa and Kobayasi[9] was used because the theory allows for an explicit expression of the film thickness and sheet cone angle with the atomizer geometry.

With the use of the potential flow theory proposed by Tanasawa and Kobayasi[9] for a swirl chamber, the cavity factor $k\ (= d_c/d_e)$ is given by the following equation:

$$K = \sqrt{1/k^2 - 1} - k \ln\left(1/k + \sqrt{1/k^2 - 1}\right) \tag{1}$$

where K is an atomizer constant that is a function of the ratio of the sectional area of the inlet to the outlet of the center post and that is determined only by the dimensions of the injector. Because the cavity factor is defined by the ratio of the diameter of the gas core and the inner diameter of the center post, the film thickness h_i is obtained as

$$h_i = (1 - k)(d_e/2) \tag{2}$$

where h_i is the initial film thickness used in the theoretical analysis. The constant liquid velocity U_i is obtained as

$$U_i = U_a \Big/ \sqrt{1 - k^2} \tag{3}$$

where U_a is the average liquid axial velocity and is given as

$$U_a = (m_l/\rho_l)(1/\pi d_e h_i) \tag{4}$$

where m_l and ρ_l are the liquid mass flow rate and the liquid density, respectively.

The momentum and continuity equations of a two-dimensional boundary layer are given as follows:

$$u\frac{\partial u}{\partial x} + v\frac{\partial u}{\partial y} = \nu_l \frac{\partial^2 u}{\partial y^2} \tag{5}$$

$$\frac{\partial u}{\partial x} + \frac{\partial v}{\partial y} = 0 \tag{6}$$

where ν_l is the liquid kinematic viscosity and u and v the liquid velocities in the x and y directions, respectively. The boundary conditions at $y = 0$ are given as

$$u = v = 0 \tag{7}$$

and at $y = h$ are

$$\frac{\partial u}{\partial y} = 0 \tag{8}$$

The liquid volumetric flow rate per unit width, Q, is defined as

$$Q = \int_0^h u \, \mathrm{d}y \tag{9}$$

The velocity u can be expressed as follows using the film surface velocity U:

$$u = U(x) \cdot f(\eta) \tag{10}$$

where $f(\eta)$ is the velocity distribution across the boundary layer and is given by the following equation for a laminar boundary layer[8]:

$$f(\eta) = 2\eta - 2\eta^3 + \eta^4 \tag{11}$$

where η indicates the nondimensional y coordinate, that is, y/h. The velocity distribution across the turbulent boundary layer is given by the one-seventh power law as

$$f(\eta) = \eta^{\frac{1}{7}} \tag{12}$$

At the transition from laminar to turbulence, it was assumed that the momentum of the liquid film is conserved. The Reynolds number of the boundary layer is defined as

$$Re_x = U_i x/\nu_l \tag{13}$$

The transition to turbulence at $Re_{x\,\mathrm{crit}} = 1.0 \times 10^5$ was determined by comparing the calculated and measured film thickness.

The solution to Eqs. (5) and (6) has several branches, depending on the location between $x = x_0$, where the laminar boundary layer reaches the film surface, and $x = x_t$, where the transition to turbulence occurs.

A. Case $x_0 < x_t$

$x < x_0$

The momentum integral equation of a boundary layer is given by

$$\frac{\mathrm{d}}{\mathrm{d}x}\int_0^\delta \left(U_i u - u^2\right) \mathrm{d}y = \frac{\tau_w}{\rho_l} \tag{14}$$

where

$$\tau_w = \rho_l \nu_l \left(\frac{\partial u}{\partial y}\right)_{y=0} \tag{15}$$

In this region, $U(x)$ in Eq. (10) equals U_i. Substitution of Eqs. (10) and (11) into Eq. (14) and application of the boundary condition that $\delta = 0$ at $x = 0$ give the following equation for the boundary layer thickness:

$$\delta^* = 5.84\sqrt{x^*/Re} \tag{16}$$

where δ^* and x^* are the nondimensional boundary-layer thickness and streamwise distance from the inlet normalized by h_i, respectively. The Reynolds number Re is defined as

$$Re = h_i U_i/\nu_l \tag{17}$$

The continuity equation gives

$$Q = U_i h_i = \int_0^\delta u \, \mathrm{d}y + U_i(h - \delta) \tag{18}$$

Substitution of Eqs. (10) and (11) into Eq. (18) gives

$$Q = (7/10)U_i\delta + U_i(h-\delta) = U_i[h-(3/10)\delta] \tag{19}$$

Thus, the film thickness h is given as

$$h^* = 1 + (3/10)\delta^* \tag{20}$$

where h^* is the nondimensional film thickness normalized by h_i. Furthermore, $h=\delta$ at $x=x_0$. Thus, from Eqs. (16) and (20), the following equation is deduced:

$$x_0^* = 0.0598Re \tag{21}$$

$x_0 < x < x_t$

In this region, the boundary layer occupies the whole liquid film. The momentum integral equation is given by

$$\frac{\mathrm{d}}{\mathrm{d}x}\int_0^h u^2\,\mathrm{d}y = -\frac{\tau_w}{\rho_l} \tag{22}$$

where

$$\tau_w = \rho_l \nu_l \left(\frac{\partial u}{\partial y}\right)_{y=0}$$

The continuity equation gives

$$Q = U_i\, h_i = \int_0^h u\,\mathrm{d}y = \frac{7}{10}Uh \tag{23}$$

Substitution of Eqs. (10) and (11) into Eqs. (22) and (23) leads to

$$\frac{\mathrm{d}U}{\mathrm{d}x} = -1.682\frac{\nu_l U^2}{Q^2} \tag{24}$$

Since $U=U_i$ at $x=x_0$,

$$U^* = 1\Big/\left[1 + A\left(x^* - x_0^*\right)\right] \tag{25}$$

where U^* is the nondimensional film surface velocity normalized by U_i and A is defined as

$$A = 1.682(\nu_l/Q) \tag{26}$$

Substitution of $Q=U_ih_i$ into Eq. (23) gives

$$U^*h^* = 10/7 \tag{27}$$

Manipulation of Eqs. (25) and (27) gives the following equation for the liquid-film thickness:

$$h^* = 1.429\left\{1 + A\left(x^* - x_0^*\right)\right\} \tag{28}$$

$x_t < x$

According to assumption 3, the velocity distribution across the turbulent boundary layer is given by Eq. (12). The continuity equation leads to

$$Q = U_ih_i = \int_0^h u\,\mathrm{d}y = \frac{7}{8}Uh \tag{29}$$

The wall shear stress on a flat plate for a turbulent boundary layer flow is given by

$$\tau_w = 0.0225\rho_l U^2(\nu_l/Uh)^{\frac{1}{4}} \tag{30}$$

Substitution of Eqs. (12) and (30) into Eqs. (22) and (29) gives

$$\frac{\mathrm{d}U}{\mathrm{d}x} = -0.02448\frac{h_i}{U_i^3}\frac{U^2}{Re^{\frac{1}{4}}} \tag{31}$$

Substitution of U obtained by integrating Eq. (31) into Eq. (29) results in

$$h^* = 0.02798\left(x^*\Big/Re^{\frac{1}{4}}\right) + C_1 \tag{32}$$

From assumption 7, the momentum of the laminar boundary layer equals that of its turbulent counterpart at $x=x_t$. Thus,

$$C_1 = 1.429\left\{1 + A\left(x_t^* - x_0^*\right)\right\} - 0.02798\left(x_t^*\Big/Re^{\frac{1}{4}}\right) \tag{33}$$

Substitution of $Q=U_ih_i$ into Eq. (29) gives

$$U^*h^* = 8/7 \tag{34}$$

B. Case $x_t < x_0$

$x < x_t$

The film thickness is given by Eq. (20).

$x_t < x < x_0$

Substitution of Eqs. (10), (12), and (30) into Eq. (14) gives

$$\delta^{*\frac{5}{4}} = 0.2893\left(x^*\Big/Re^{\frac{1}{4}}\right) + C_2 \tag{35}$$

The assumption that the momentum of the liquid film is preserved across the transition from the laminar to turbulent boundary layer leads to

$$C_2 = 20.52\left(x_t^*\Big/Re\right)^{\frac{5}{8}} - 0.2893\left(x_t^*\Big/Re^{\frac{1}{4}}\right) \tag{36}$$

The continuity equation gives

$$Q = U_ih_i = \int_0^\delta u\,\mathrm{d}y + U_i(h-\delta) = U_i\left(h - \frac{1}{8}\delta\right)$$

Thus,

$$h^* = 1 + (1/8)\delta^* \tag{37}$$

Because the film thickness equals the boundary-layer thickness at $x=x_0$, the following equation is obtained:

$$x_0^* = [(1.182 - C_2)/0.2893]Re^{\frac{1}{4}} \tag{38}$$

$x_0 < x$

Substitution of Eqs. (10), (12), and (30) into Eq. (22) gives

$$h^* = 0.02798\left(x^*\Big/Re^{\frac{1}{4}}\right) + C_3 \tag{39}$$

Now $h=\delta$ at $x=x_0$. Use of Eqs. (33), (34), and (36), gives the following equation:

$$C_3 = 1.143 - 0.02798\left(x_0^*\Big/Re^{\frac{1}{4}}\right) \tag{40}$$

The continuity equation gives

$$Q = U_ih_i = \int_0^h u\,\mathrm{d}y = \frac{7}{8}Uh$$

Thus,

$$U^*h^* = 8/7 \tag{41}$$

The sheet cone angle 2α is given by

$$2\alpha = 2\tan^{-1}\left\{k\Big/\sqrt{1-k^2}\right\} \tag{42}$$

Equation (42) was derived from the potential flow theory of Tanasawa and Kobayasi[9] and should be corrected using the Reynolds number and the center post length. Based on the preceding discussion, the following empirical equation for the sheet cone angle was proposed by trial and error:

$$2\alpha_R = 2\alpha\left(a\Big/\sqrt{L/h_i\cos\alpha}\right)\exp(-b/Re) \tag{43}$$

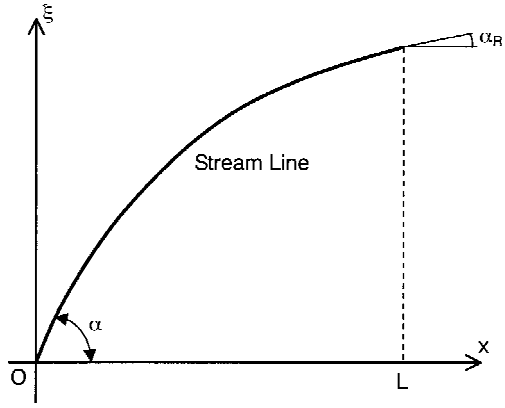

Fig. 4 Streamline.

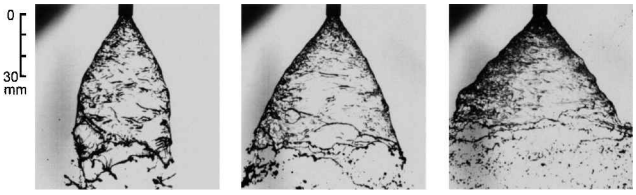

a) $m_l = 26.1$ **g/s** **b)** $m_l = 32.5$ **g/s** **c)** $m_l = 48.6$ **g/s**

Fig. 5 Disintegration phenomena of hollow cone sheet, $L/d_e = 11.67$.

where L indicates the center post length. Here a and b are empirical constants determined by comparing Eq. (43) with measurements. They have values of 18.9 and 670, respectively, in the present study. For other injector geometries, a and b may have the different values.

The liquid entering the center post flows toward the exit along a spiral streamline, which can be approximated by a quadratic equation shown in Fig. 4, wherer ξ is the azimuthal coordinate on the inner wall of the center post. The orientation of the streamline is α at $x = 0$ and α_R at $x = L$. Therefore, the streamline can be expressed by

$$x = p\xi^2 + q\xi \tag{44}$$

$$p = (1/4L)\left(1/\tan^2\alpha_R - 1/\tan^2\alpha\right) \tag{45}$$

$$q = 1/\tan\alpha \tag{46}$$

The distance from $x = 0$ along the streamline, L_x, can be expressed by

$$L_x = \int_0^{2L[\tan\alpha\cdot\tan\alpha_R/(\tan\alpha+\tan\alpha_R)]} \sqrt{(2p\xi+q)^2+1}\,\mathrm{d}\xi \tag{47}$$

Han et al. proposed a semi-empirical equation for the breakup length L_{bu} of the conical sheet from a swirl atomizer.[11] That model is revised to provide better agreement with measurements conducted in the present work:

$$L_{\mathrm{bu}} = B\left\{\frac{\rho_l\sigma\,\ell_n(\zeta/\zeta_0)h_0\cos\alpha}{\rho_g^2 U_0^2}\right\}^{0.3} \tag{48}$$

where σ and ρ_g are the surface tension and gas density, respectively. Here ζ is the wave amplitude when the sheet breaks up, and the parameter $\ell_n(\zeta/\zeta_0)$ was determined to be equal to 12 according to Han et al.[11] B is the experimental constant, determined experimentally to be equal to 0.2175. U_0 is the liquid–gas relative velocity at the exit.

IV. Results and Discussion

A. Disintegration Phenomenon of Swirling Hollow Cone Sheet

Figure 5 shows the disintegration phenomenon of the conical sheet issued from the injector. Nitrogen gas is not injected. The conical sheet fluctuates vigorously and disintegrates into ligaments and droplets at the sheet tip. The sheet cone angle increases as the liquid flow rate increases due to the increase of the liquid momentum. The sheet breakup point approaches the injector as the liquid flow rate increases.

B. Film Thickness

Figures 6 shows the measured azimuthal distributions of the local film thickness at the center post exit. As shown in Fig. 1, θ of the abscissa indicates the azimuthal angle. The film thickness fluctuates in the azimuthal direction and has three peaks corresponding to the number of water inlet holes. The azimuthal locations of the peaks change according to the liquid flow rate. The width of the thickness fluctuations is from 0.2 to 0.4 mm.

Figure 7 shows the comparison of the average film thickness between the theoretical analysis and the measurements. First, the film thickness decreases monotonically as the water flow rate increases until 10 g/s. At liquid flow rates greater than 10 g/s, the film thickness shows almost the same values. A small decrease of the film thickness is observed at around $m_l = 20$ g/s. This may be attributed to the transition from laminar to turbulence that occurs before the boundary layer reaches the film surface. Because it was assumed that the momentum of the liquid film is conserved at transition, in the case of $x_t < x_0$, the liquid-film thickness is discontinuous at the transition.

The effect of the center post length on the average film thickness at the tube exit is shown in Fig. 8. The average film thickness increases lineally with increasing post length due to the liquid momentum loss between the inlet and the exit. Figure 9 shows the change of film thickness along the x axis. The film thickness increases as the liquid

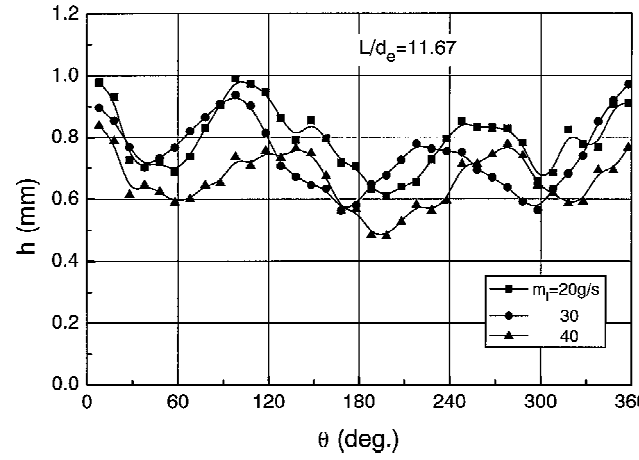

Fig. 6 Azimuthal distributions of local film thickness at center post exit.

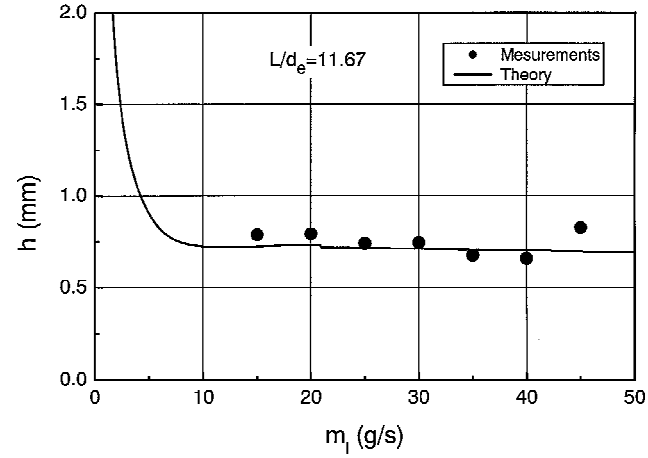

Fig. 7 Effects of liquid flow rate on average film thickness.

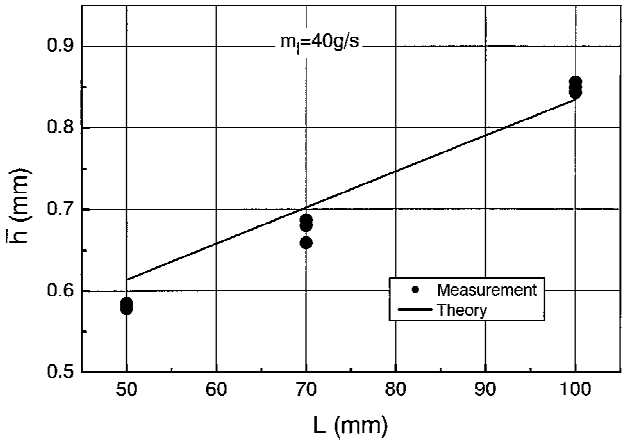

Fig. 8 Average film thickness at center post exit.

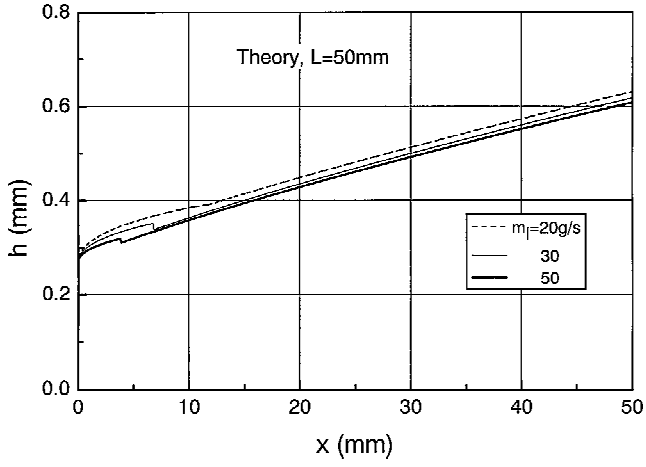

Fig. 9 Predicted film thickness vs distance from inlet.

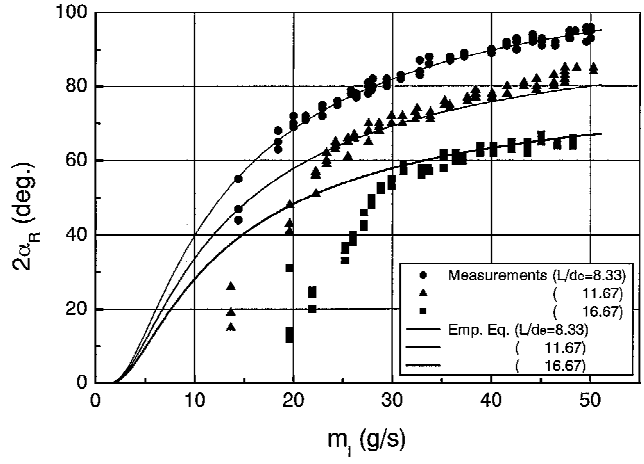

Fig. 10 Comparison of measured sheet cone angle and empirical equation.

moves downstream. However, for $m_l = 20$ g/s, the rate of increase changes at around $x = 12$ mm, which corresponds to the transition to turbulence in the case of $x_0 < x_t$. For $m_l = 30$ and 50 g/s, sudden decreases of the film thickness are observed at around $x = 7$ and 3 mm, respectively, because of the transitions in the case of $x_t < x_0$, as mentioned earlier.

C. Sheet Cone Angle

The effect of liquid flow rate on sheet cone angle is shown in Fig. 10. The empirical equations agree with the measurements for

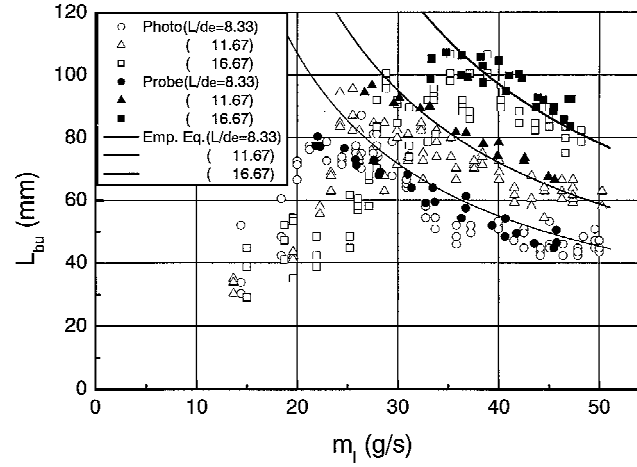

Fig. 11 Comparison of measured sheet breakup length and empirical equation.

cone angles larger than 55 deg. The discrepancies for small cone angles seem to be due to the effect of surface tension. When the tangential momentum of the liquid is small, the conical sheet is deflated by the surface tension in the azimuthal direction, and the cone angle decreases. The effect is more profound for small cone angles. The liquid flow rates at which the cone angle decreases rapidly with the decrease of the liquid flow rate are 15 g/s for $L/d_e = 8.33$, 22 g/s for $L/d_e = 11.67$, and 30 g/s for $L/d_e = 16.67$.

D. Sheet Breakup Length

Figure 11 shows the comparison of the measurements and the empirical equations for the sheet breakup length. Solid symbols indicate the measurements by the contact mesh probe and the open symbols by the instantaneous photographs. The breakup lengths measured by the probe are slightly larger than those shown by the photographs. The empirical equations are almost coincident with the probe measurements except for small liquid flow rates. In general, the breakup length of a liquid sheet shows the same trend as that in Fig. 11. At a small film Reynolds number, the liquid flow is laminar, and the breakup length increases with the increase of the film injection velocity. On the other hand, at a large film Reynolds number, the liquid flow becomes turbulent, and the breakup length decreases with the increase of the film injection velocity. Therefore, the empirical equation of the breakup length proposed in the present work can be applied to turbulent liquid films. The liquid flow rates at which the breakup length reaches its maximum are 22 g/s for $L/d_e = 8.33$, 27 g/s for $L/d_e = 11.67$, and 34 g/s for $L/d_e = 16.67$.

E. Spray Characteristics

The mean droplet size and droplet velocity were measured by means of a phase Doppler particle analyzer. The measurements were carried out at several azimuths. No meaningful difference was observed in spite of the variations of the film thickness in the azimuthal direction.

Figure 12 shows the radial profiles of the Sauter mean diameter (SMD) at three axial distances from the injector exit. The mean droplet size decreases in all of the cases and then increases toward the spray periphery. In the spray center portion, the static pressure is lower than that in the periphery due to the nitrogen injection from the annular gap. Thus, small droplets gather at the center and then coalesce with each other. This results in an increase of the mean droplet size in the center. On the other hand, large droplets penetrate the spray in the direction of the initial sheet cone angle due to their large inertia, thereby leading to an increase of the mean droplet size in the periphery.

Figure 13 shows the effects of the gas flow rate on SMD in the center. As the gas mass flow rate increases, the mean diameter decreases monotonically, and the larger the liquid flow rate is, the larger the mean diameter is. This trend bears a close resemblance to that of conventional airblast atomizers.

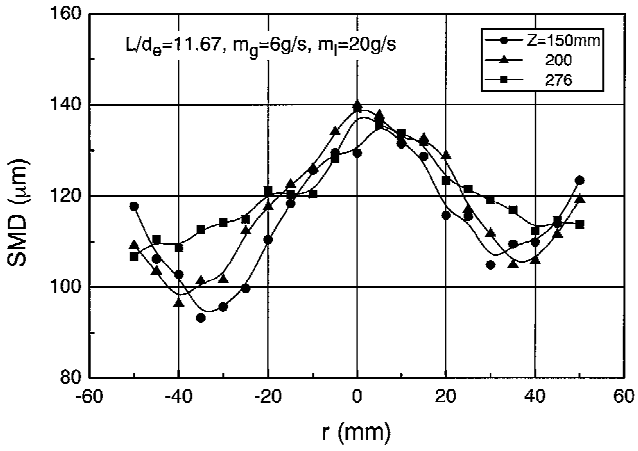

Fig. 12 Radial profile of mean droplet size.

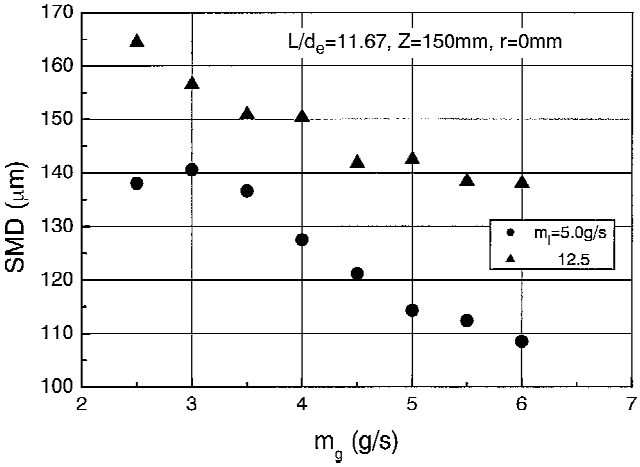

Fig. 13 Effect of gas flow rate on mean droplet size.

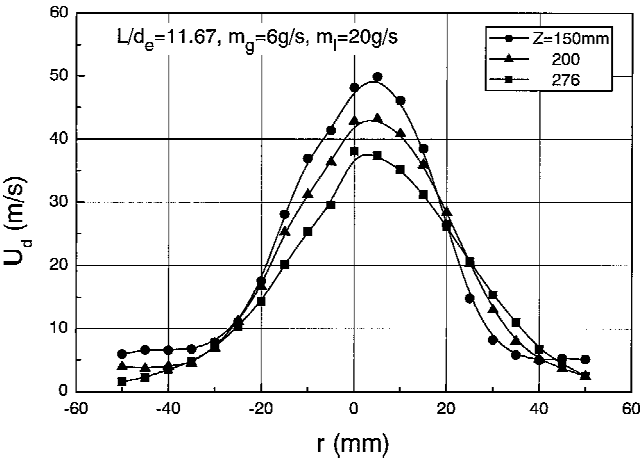

Fig. 14 Radial profile of average droplet velocity.

For airblast atomization of a liquid film, Rizk and Lefebvre reported that SMD is proportional to the 0.4 power of the film thickness in a coflow-type airblast atomizer.[4] Inamura and Nagai reported that SMD is proportional to the film thickness in an impinge-type airblast atomizer.[5] In both cases, the larger the film thickness is, the larger SMD is. From the theoretical analysis shown in Fig. 7, the film thickness at $m_l = 5.0$ g/s is slightly larger than that at $m_l = 12.5$ g/s. In Fig. 13, SMD at $m_l = 5.0$ g/s is smaller than that at $m_l = 12.5$ g/s. This discrepancy occurs because the measurement point of the drop size is located only at the center and SMD is affected not only by the film thickness, but also by the other injection conditions, such as

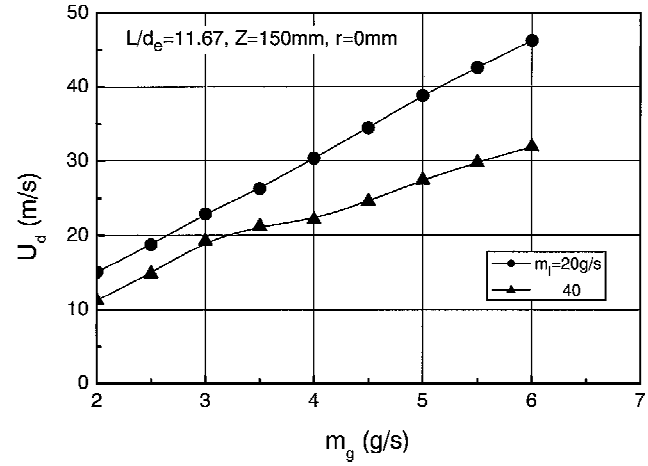

Fig. 15 Effect of gas flow rate on average droplet velocity.

air-to-liquid mass flow rate ratio.[12] To clarify the effects of injection conditions on SMD, further studies should be conducted.

Figure 14 shows the radial profiles of the average droplet velocity, exhibiting the kind of normal distribution typical of a circular compound jet.[13] As the measurement point moves downstream, the peak of the profile becomes low, and the profile approaches a flat one.

Figure 15 shows the effects of the gas flow rate on the average droplet velocity in the center. The average droplet velocity increases linearly with the gas flow velocity. The larger the liquid flow rate is, the larger the rate of the increase is of the average droplet velocity. This trend is similar to that of a circular compound jet.[13]

V. Conclusions

The flow evolution in the center post of a swirl injector was investigated theoretically using a boundary-layer theory. The predicted film thickness at the post exit was compared with measurements for three different post lengths. The theoretical analysis showed good agreement with experimental data except for small liquid flow rates, at which the measured film thickness increases rapidly compared with the theoretical predictions as the flow rate decreases.

Empirical correlations for the sheet cone angle and breakup length were deduced for cases without gasstream injection. The measured sheet cone angle and breakup length deviate from the empirical equations for small liquid flow rates because the liquid film transits from turbulence to laminar as the liquid flow rate decreases. The empirical equation of the breakup length proposed in this paper can be applied to turbulent films.

The mean droplet size shows a nonuniform distribution in the radial direction, reaching local maxima at the center and periphery. The radial profile of the average droplet velocity shows a normal distribution, typical of a circular compound jet.

Acknowledgments

The authors would like to thank K. Miyata and H. Senba of Hirosaki University for their help during the experiments.

References

[1]Rahman, S., Pal, S., and Santoro, R. J., "Swirl Coaxial Atomization: Cold-Flow and Hot-Fire Experiments," AIAA Paper 95-0381, July 1995.

[2]Tamura, H., Sakamoto, H., Takahashi, M., Sasaki, M., Tomita, T., and Nagao, R., "LOX/LH2 Subscale Swirl Coaxial Injector Testing," AIAA Paper 97-2906, July 1997.

[3]Feikema, D. A., Eskridge, R., and Hutt, J. J., "Structure of a Nonevaporating Swirl Injector Spray," *Atomization and Sprays*, Vol. 7, No. 1, 1997, pp. 77–95.

[4]Rizk, N. K., and Lefebvre, A. H., "The Influence of Liquid Film Thickness on Airblast Atomization," *Journal of Engineering for Power*, Vol. 102, No. 3, 1980, pp. 706–710.

[5]Inamura, T., and Nagai, N., "The Relative Performance of Externally and Internally-Mixed Twin-Fluid Atomizers," *Proceedings of the 3rd*

International Conference on Liquid Atomization and Spray Systems, The Inst. of Energy, London, 1985, pp. IIC/2/1–IIC/2/11.

[6]Tokuoka, N., Nagaosa, S., Hora, S., and Sato, G. T., "Study on the Disintegration of a Liquid Film by Air Impingement," *Atomization and Spray Technology*, Vol. 1, No. 2, 1985, pp. 103–123.

[7]Hiroyasu, H., Shimizu, M., and Arai, M., "The Break-Up of High Speed Jet in a High Pressure Gaseous Atmosphere," *Proceedings of the 2nd International Conference on Liquid Atomization and Spray Systems*, The Inst. of Energy, London, 1982, pp. 69–76.

[8]Ishigai, K., Nakanishi, S., Mizuno, M., and Imamura, T., "Heat Transfer by Impingement of Round Water Jet," *Transactions of the Japan Society of Mechanical Engineers*, Ser. 2, Vol. 42, No. 357, 1976, pp. 1502–1510 (in Japanese).

[9]Tanasawa, Y., and Kobayasi, K., "A Study on Swirl Atomizer," *Technical Report of Tohoku University*, Vol. 20, No. 1, 1955, pp. 27–58.

[10]Rizk, N. K., and Lefebvre, A. H., "Internal Flow Characteristics of Simplex Swirl Atomizers," *Journal of Propulsion and Power*, Vol. 1, No. 3, 1985, pp. 193–199.

[11]Han, Z., Parrish, S., Farrell, P. V., and Reitz, R. D., "Modeling Atomization Processes of Pressure-Swirl Hollow-Cone Fuel Sprays," *Atomization and Sprays*, Vol. 7, No. 6, 1997, pp. 663–684.

[12]Lefebvre, A. H., *Atomization and Sprays*, Hemisphere, New York, 1989, Chap. 6.

[13]Rajaratnam, N., *Turbulent Jets*, Elsevier Scientific, New York, 1976, Chap. 4.